SIAM J. Applied Dynamical Systems
Vol. 20, No. 4, pp. 2391–2411

Interpolatory Methods for Generic BizJet Gust Load Alleviation Function*

Charles Poussot-Vassal†, Pierre Vuillemin†, Olivier Cantinaud‡, and Florian Sève‡

Abstract. The paper's main contribution concerns the use of interpolatory methods to solve end-to-end industrial control problems involving complex linear dynamical systems. In more detail, contributions show how rational function interpolation is a pivotal tool (i) to construct (frequency-limited) reduced-order dynamical models appropriate for model-based control design and (ii) to accurately discretize controllers in view of onboard computer-limited implementation. These contributions are illustrated along the paper through the design of an active feedback gust load alleviation function, applied on an industrial generic business jet aircraft use case. The closed-loop validation and performance evaluation are assessed through the use of a dedicated industrial simulator and considering certification objectives. Although application is centered on aircraft applications, the method is not restrictive and can be applied to any linear dynamical system.

Key words. rational interpolation, discretization, sampled-time control, time-delayed systems, model approximation, gust load control

AMS subject classifications. 01-08, 35B30, 41A20, 41A63, 93A15, 93A30, 93B15, 93B52, 93C35, 93C57, 93C62, 93C80, 93C95

DOI. 10.1137/20M1384014

1. Introduction.

1.1. General aircraft context.

Aircraft mobility plays an important role in our lifestyle and societal organization. As this transportation means is facing severe environmental and societal challenges (e.g., global warming and CO_2 emissions), it is the role of researchers to provide innovative answers and industry-oriented tools to address them. These solutions should fulfill the safety and design requirements and be numerically efficient and simple to implement within the aircraft industrial design value chain. Among other scientific disciplines, it is well admitted that the civil aircraft industry relies on dynamical systems theory, linear algebra, and computational sciences to address these issues. In light of these statements, recent developments in these scientific communities may have a major impact on the overall aircraft conception and exploitation enhancement. Within the aeroelastic field, one may mention efforts in modeling and gust load alleviation (GLA) [29, 28], vibration reduction [23], and flutter detection [30, 24]. In other aircraft fields, one should also mention [2, 41], given the

*Received by the editors December 3, 2020; accepted for publication (in revised form) by I. Belykh September 1, 2021; published electronically November 22, 2021.
https://doi.org/10.1137/20M1384014
Funding: This work was supported within the frame of the Joint Technology Initiative JTI Clean Sky 2, AIRFRAME Integrated Technology Demonstrator platform AIRFRAME ITD (contract no. CSJU-CS2-GAM-AIR-2014-15-01 Annex 1, Issue B04, October 2nd, 2015) being part of the Horizon 2020 research and Innovation framework program of the European Commission.
†ONERA, 31055, Toulouse, Cedex, France (charles.poussot-vassal@onera.fr, pierre.vuillemin@onera.fr).
‡Dassault-Aviation, 92 552, Saint-Cloud, Cedex, France (Olivier.Cantinaud@dassault-aviation.com, Florian.Seve@dassault-aviation.com).

strong connection with this work. Authors believe that related computational methods and tools can lead to important improvements in the *civil aviation footprint reduction*. This is one of the main objectives of this work.

In order to reach these objectives, the paper highlights the pivotal role and relevance of *interpolatory methods* [4, 5] in the context of *linear time invariant (**LTI**) large-scale systems* [31].

1.2. Generic business jet aircraft context and industrial constraints. Through a complete industrial GLA control design and validation problem applied to a generic business jet aircraft, we show how rational function interpolation is a central ingredient for engineers. It is used (i) to construct *a reduced-order dynamical models* appropriate for feedback control function design and (ii) to accurately *discretize* a linear dynamical controller in view of constrained onboard computer implementation. The complete closed-loop stability and performance analysis is done through a dedicated *industrial simulator* to assess the approach.

In an industrial value chain, the GLA function, which targets load reduction along wings in response to gust disturbances, is designed after the flight controller (focusing on handling qualities). Consequently, one additional requirement of GLA control is to keep nominal (low frequencies) flight performances unchanged and focus on the gust phenomena and load envelope only. In addition, as the control functions should be implemented in a limited sampled-time computer, with a constrained material architecture (sensor and actuator limitations, sampling limitations, delays in the loop, etc.), the discretization step should also be accurately taken into account before any implementation and performance evaluation.

1.3. Paper organization and principal contributions. Given the above considerations and objectives, the rest of the paper is focused on the central role of the *interpolation* applied to the *GLA control* problem and on the new development of an interpolatory-driven discretization method. Reminders on the interpolation framework are first given in section 2. The gust load–oriented aircraft (medium-scale) *irrational modeling* is detailed in section 3. Its rational and reduced approximation, leading to models suitable for linear control design, is illustrated in section 4. Then, after briefly describing the continuous-time GLA controller synthesis, the controller *discretization* through the interpolation framework is detailed in section 5. Finally, conclusions are given in section 6, first to illustrate the efficiency of the proposed process to alleviate gust loads in an industrial application context and then to discuss the obtained results.

The global contribution of this article lies in the use of interpolatory methods in the development of an end-to-end solution to solve an industrial aeronautical problem (sections 3–5). This result is made possible thanks to two methodological contributions: the exact modeling of the gust impact over an aeroelastic aircraft model (section 3) followed by an appropriate approximation (section 4) and the interpolatory-based discretization scheme (section 5). Although the paper is centered around the aircraft gust load function, the overall approach is also valid to (m)any linear time invariant dynamical systems. Moreover, the presented interpolatory-based discretization method of section 5 may be applied to any linear time invariant continuous-time model.

1.4. Notations. Let us denote by $\mathbb{R}$ the set of real numbers, $\mathbb{C}$ the set of complex numbers, $\mathbb{C}_+$ ($\mathbb{C}_-$) the open right (left) half-plane, $\mathcal{D}$ the open unit disk, $\partial\mathcal{D}$ its boundary, and $\overline{\mathcal{D}}$ the complementary of the closed unit disk, respectively. The complex variable is given by $\imath = \sqrt{-1}$. Let $\mathcal{L}_2(\mathcal{I})$ ($\mathcal{I} = \imath\mathbb{R}$ or $\partial\mathcal{D}$) be the set of functions that are square integrable on $\mathcal{I}$. Let $\mathcal{H}_2(\mathcal{D})$ (resp., $\mathcal{H}_2(\overline{\mathcal{D}})$) be the subset of $\mathcal{L}_2(\partial\mathcal{D})$ containing the functions analytic in $\mathcal{D}$ (resp., $\overline{\mathcal{D}}$). Let $\mathcal{H}_2(\mathbb{C}_+)$, shortly $\mathcal{H}_2$ (resp., $\mathcal{H}_2(\mathbb{C}_-)$), be the subset of $\mathcal{L}_2(\imath\mathbb{R})$ containing the functions analytic in $\mathbb{C}_+$ (resp., $\mathbb{C}_-$). Similarly, let $\mathcal{L}_\infty(\mathcal{I})$ ($\mathcal{I} = \imath\mathbb{R}$ or $\partial\mathcal{D}$) be the set of functions that are bounded on $\mathcal{I}$. Let $\mathcal{H}_\infty(\mathcal{D})$ (resp., $\mathcal{H}_\infty(\overline{\mathcal{D}})$) be the subset of $\mathcal{L}_\infty(\partial\mathcal{D})$ containing the functions analytic in $\mathcal{D}$ (resp., $\overline{\mathcal{D}}$) and $\mathcal{H}_\infty(\mathbb{C}_+)$, shortly $\mathcal{H}_\infty$, the subset of $\mathcal{L}_\infty(\imath\mathbb{R})$ of functions analytic in $\mathbb{C}_+$. The Fourier transform of a time-domain signal $v \in \mathcal{L}_2(\mathbb{R})$ is denoted by $\overline{v} = \mathcal{F}(v)$.

2. Preliminaries in rational interpolation and approximation.

The entire proposal relies on a specific use of the model interpolation tools, namely, the *Loewner* and the *optimal (frequency-limited) $\mathcal{H}_2$ frameworks*. In this section, the Loewner framework is recalled in its general form in subsection 2.1. Then $\mathcal{H}_2$ model order dimension reduction methods are recalled in subsections 2.2–2.4.

2.1. Reminder of the Loewner framework. The main elements of the Loewner framework are recalled in the multi-input multi-output (**MIMO**) general square case. For a complete description, readers may refer to [5, 22] and to [3] for insight in the rectangular case. Under mild considerations, the Loewner approach is a data-driven method aimed at building a rational descriptor **LTI** dynamical model $\mathbf{H}^m$ of dimension m which interpolates given complex data, here generated by an underlying "unknown" model $\mathbf{H}$. Let us be given the left or row data and the right or column data,

$$\left.\begin{array}{c}(\mu_j, \mathbf{l}_j^H, \mathbf{v}_j^H)\\ \text{for } j = 1, \dots, m\end{array}\right\} \quad \text{and} \quad \left\{\begin{array}{c}(\lambda_i, \mathbf{r}_i, \mathbf{w}_i)\\ \text{for } i = 1, \dots, m,\end{array}\right. \tag{2.1}$$

where $\mathbf{v}_j^H = \mathbf{l}_j^H \mathbf{H}(\mu_j)$ and $\mathbf{w}_i = \mathbf{H}(\lambda_i)\mathbf{r}_i$, with $\mathbf{l}_j \in \mathbb{C}^{n_y \times 1}$, $\mathbf{r}_i \in \mathbb{C}^{n_u \times 1}$, $\mathbf{v}_j \in \mathbb{C}^{n_u \times 1}$, and $\mathbf{w}_i \in \mathbb{C}^{n_y \times 1}$. The $\mathbf{w}_i$ and $\mathbf{v}_j$ are the complex measurement data at the points $\mu_j \in \mathbb{C}$ and $\lambda_i \in \mathbb{C}$, along the tangential directions $\mathbf{l}_j$ and $\mathbf{r}_i$. We denote $\{z_k\}_{k=1}^{2m} = \{\mu_j\}_{j=1}^{m} \cup \{\lambda_i\}_{i=1}^{m}$ as the interpolation (or support) points. The method then consists in building the *Loewner* $\mathbb{L} \in \mathbb{C}^{m \times m}$ and *shifted Loewner* $\mathbb{L}_\sigma \in \mathbb{C}^{m \times m}$ matrices defined as follows for $i, j = 1, \dots, m$:

$$[\mathbb{L}]_{j,i} = \frac{\mathbf{v}_j^H \mathbf{r}_i - \mathbf{l}_j^H \mathbf{w}_i}{\mu_j - \lambda_i} \quad \text{and} \quad [\mathbb{L}_\sigma]_{j,i} = \frac{\mu_j \mathbf{v}_j^H \mathbf{r}_i - \lambda_i \mathbf{l}_j^H \mathbf{w}_i}{\mu_j - \lambda_i}. \tag{2.2}$$

Then the model $\mathbf{H}^m$ given by the following descriptor realization $\mathcal{S}^m$:

$$E^m \delta\{\mathbf{x}(\cdot)\} = A^m \mathbf{x}(\cdot) + B^m \mathbf{u}(\cdot) \quad \text{and} \quad \mathbf{y}(\cdot) = C^m \mathbf{x}(\cdot), \tag{2.3}$$

where $E^m = -\mathbb{L}$, $A^m = -\mathbb{L}_\sigma$, $[B^m]_k = \mathbf{v}_k^H$ and $[C^m]_k = \mathbf{w}_k$ (for $k = 1, \dots, m$) and whose related transfer function $\mathbf{H}^m(\xi) = C^m (\xi E^m - A^m)^{-1} B^m$ interpolates $\mathbf{H}$ at the given driving frequencies and directions defined in (2.1), i.e., satisfies

$$\mathbf{l}_j^H \mathbf{H}^m(\mu_j) = \mathbf{l}_j^H \mathbf{H}(\mu_j) \quad \text{and} \quad \mathbf{H}^m(\lambda_i)\mathbf{r}_i = \mathbf{H}(\lambda_i)\mathbf{r}_i. \tag{2.4}$$

Remark 2.1 (about $\delta\{\cdot\}$ and ξ notations). In (2.3), "$(\cdot)$" denotes the considered time-domain variable; this latter can either be "(t)" for continuous-time models ($t \in \mathbb{R}_+$) or "$[q]$" for sampled-time models ($q \in \mathbb{Z}$). Similarly, in (2.3), "$\delta\{\cdot\}$" stands as the shift operator being either $\delta\{\mathbf{x}(t)\} = \dot{\mathbf{x}}(t)$ in the continuous-time case and $\delta\{\mathbf{x}(q)\} = \mathbf{x}[q+1]$ in the sampled-time one. Moreover, ξ stands as the associated complex version being the Laplace variable $\xi = s$ in the continuous-time case and the forward shift $\xi = z$ in the sampled-time one.

Assuming that the number $2m$ of available data is large enough, it has been shown in [22] that a minimal model $\mathbf{H}^n$ of dimension $n < m$ that still interpolates the data can be built with a projection of (2.3) provided that, for $k = 1, \ldots, 2m$,

$$\mathbf{rank}\,(z_k\mathbb{L} - \mathbb{L}_\sigma) = \mathbf{rank}\,([\mathbb{L}, \mathbb{L}_\sigma]) = \mathbf{rank}\left([\mathbb{L}^H, {\mathbb{L}_\sigma}^H]^H\right) = n. \tag{2.5}$$

Then let us denote $Y \in \mathbb{C}^{m\times n}$ the matrix containing the first n left singular vectors of $[\mathbb{L}, \mathbb{L}_\sigma]$ and $X \in \mathbb{C}^{m\times n}$ the matrix containing the first n right singular vectors of $[\mathbb{L}^H, {\mathbb{L}_\sigma}^H]^H$. Then

$$E^n = Y^H E^m X,\ A^n = Y^H A^m X,\ B^n = Y^H B^m,\ C^n = C^m X \tag{2.6}$$

is a realization of the model $\mathbf{H}^n$ given as $\mathbf{H}^n(\xi) = C^n\,(\xi E^n - A^n)^{-1}\,B^n$, embedding a *minimal McMillan degree* equal to $\mathbf{rank}\,(\mathbb{L})$. The quadruple $\mathcal{S}^n : (E^n, A^n, B^n, C^n)$ is a descriptor realization of $\mathbf{H}^n$. Note that if n in (2.5) is greater than $\mathbf{rank}(\mathbb{L})$, then $\mathbf{H}^n$ can either have a direct-feedthrough or a polynomial part. The reader may note that the number n of singular vectors composing Y and X used to project the system $\mathbf{H}^n$ in (2.6) may be decreased even further at the cost of approximate interpolation of the data. This allows for a trade-off between complexity of the resulting model and accuracy of the interpolation. In this work, we will always consider exact interpolation, while the model reduction step, recalled in subsection 2.2, will be performed by (frequency-limited) $\mathcal{H}_2$-oriented interpolatory methods instead. These latter are discussed in subsections 2.3 and 2.4.

Remark 2.2 (assumptions for model order reduction). In what follows, we assume stable, strictly proper with semisimple poles $\mathbf{H}^n$. These assumptions can be theoretically removed but at the cost of a more complicated developments not appropriate in our gust load setting.

2.2. Model dimension reduction. Given the finite nth-order function $\mathbf{H}^n$ equipped with a realization defined by the quadruple $\mathcal{S}^n : (E^n, A^n, B^n, C^n)$ given in (2.6), the model reduction goal consists in constructing reduced rth-order ($r \ll n$) model $\hat{\mathcal{S}}$,

$$\hat{E}\delta\{\hat{\mathbf{x}}(\cdot)\} = \hat{A}\hat{\mathbf{x}}(\cdot) + \hat{B}\mathbf{u}(\cdot) \quad \text{and} \quad \hat{\mathbf{y}}(\cdot) = \hat{C}\hat{\mathbf{x}}(\cdot), \tag{2.7}$$

where $\hat{\mathbf{x}}(\cdot) \in \mathbb{R}^r$ are the reduced internal variables and $\hat{\mathbf{y}}(\cdot) \in \mathbb{R}^{n_y}$ is the approximated output and where $\hat{E} \in \mathbb{R}^{r\times r}$, $\hat{A} \in \mathbb{R}^{r\times r}$, $\hat{B} \in \mathbb{R}^{r\times n_u}$, and $\hat{C} \in \mathbb{R}^{n_y\times r}$ are constant matrices such that the input-output behavior of $\hat{\mathbf{H}}$ defined as $\hat{\mathbf{H}}(\xi) = \hat{C}(\xi\hat{E} - \hat{A})^{-1}\hat{B}$ is similar to $\mathbf{H}^n$; i.e., for the same input $\mathbf{u}$, the mismatch $\mathbf{y} - \hat{\mathbf{y}}$ is small in some sense.

2.3. Rational $\mathcal{H}_2$ approximation and reduction by interpolation. One way to find $\hat{\mathbf{H}}$ (or $\hat{\mathcal{S}}$) as in (2.7) is to solve the so-called $\mathcal{H}_2$ model reduction problem:[1]

$$\hat{\mathbf{H}} = \arg\min_{\mathbf{G}\in\mathcal{H}_2} ||\mathbf{H}^n - \mathbf{G}||_{\mathcal{H}_2}. \tag{2.8}$$

[1]Optimizing through the $\mathcal{H}_2$-norm is relevant, as it provides an upper bound on the worst-case time-domain error in response to an input signal [16].

The most common approach to obtain the solution of (2.8) is to work with the *first-order necessary optimality conditions* which were developed in a series of papers; see, e.g., [9, 33] for theoretical insight (see also [8] for existence and properties). The *interpolation-based* approach revisited by a sequence of contributions [13, 34, 16] resulting in an interpolatory problem is used here. In the case of semisimple poles only (see [35] for higher order poles), if $\hat{\mathbf{H}}$, equipped with a realization $\hat{\mathcal{S}} : (\hat{E}, \hat{A}, \hat{B}, \hat{C})$, is a solution of the $\mathcal{H}_2$ approximation problem (2.8), then

$$\mathbf{H}^n(\hat{\kappa}_l)\hat{\mathbf{b}}_l = \hat{\mathbf{H}}(\hat{\kappa}_l)\hat{\mathbf{b}}_l,\ \hat{\mathbf{c}}_l^H\mathbf{H}^n(\hat{\kappa}_l) = \hat{\mathbf{c}}_l^H\hat{\mathbf{H}}(\hat{\kappa}_l) \ \text{ and } \ \hat{\mathbf{c}}_i^H \left.\frac{d\mathbf{H}^n}{d\xi}\right|_{\xi=\hat{\kappa}_l} \hat{\mathbf{b}}_l = \hat{\mathbf{c}}_l^H \left.\frac{d\hat{\mathbf{H}}}{d\xi}\right|_{\xi=\hat{\kappa}_l} \hat{\mathbf{b}}_l, \tag{2.9}$$

where $[\hat{\mathbf{b}}_1, \ldots, \hat{\mathbf{b}}_r]^H = R\hat{B}$ and $[\hat{\mathbf{c}}_1, \ldots, \hat{\mathbf{c}}_r] = \hat{C}L$ and where $L \in \mathbb{C}^{r\times r}$ and $R \in \mathbb{C}^{r\times r}$ are the left and right eigenvectors associated to $\hat{\lambda}_l$, the eigenvalues of the $(\hat{E}, \hat{A})$ pair. Then, in the continuous-time case, $\hat{\kappa}_l = -\hat{\lambda}_l$, while in the discrete-time one, $\hat{\kappa}_l = 1/\hat{\lambda}_l$ $(l = 1, \ldots, r)$ [16, 10].

In [16], authors derive a Petrov–Galerkin type of projection-based approach [36], accompanied with a fixed point algorithm, celebrated as the **MIMO** iterative rational Krylov algorithm (**MIMO IRKA**), allowing reaching the optimality conditions (2.9). The solution results in a procedure with a fairly cheap computational cost, embedding linear equation resolutions for which efficient methods are available [32, 20, 17]. Details are skipped here, but readers can also refer to the book [4] or monograph [27, Chap. 2] for practical and numerical details.

2.4. Rational frequency-limited $\mathcal{H}_2$ approximation and reduction by interpolation. Similarly to the above $\mathcal{H}_2$ model approximation problem, it might be interesting to approximate over a frequency-limited range $\Omega = [0, \omega]$ $(\omega \in \mathbb{R}_+)$ only. This is the purpose of the *frequency-limited* $\mathcal{H}_2$, shortly $\mathcal{H}_{2,\Omega}$, approximation problem defined as [40, 25]

$$\hat{\mathbf{H}} = \arg\min_{\mathbf{G}\in\mathcal{H}_\infty} ||\mathbf{H}^n - \mathbf{G}||_{\mathcal{H}_{2,\Omega}}. \tag{2.10}$$

Interestingly, as in the seminal works of [16] treating the $\mathcal{H}_2$ objective, [37, Chap. 8] has shown that this problem can also be recast as an interpolatory one.

However, unlike the $\mathcal{H}_2$ interpolation conditions, the frequency-limited ones do not involve directly the transfer functions $\mathbf{H}$ and $\hat{\mathbf{H}}$ but irrational functions $\mathbf{T}^n_\omega(\mathbf{H})$ and $\hat{\mathbf{T}}_\omega(\hat{\mathbf{H}})$, parametrized by $\mathbf{H}$ and $\hat{\mathbf{H}}$. Here again, these functions should match at images of the poles of the reduced-order model (see details in [37, Chap. 8]). These interpolatory conditions are difficult to practically exploit. Indeed, no Krylov-like subspace has been clearly identified yet. Consequently, a **MIMO IRKA** type pf procedure as in [16] is not straightforward to develop.[2] So far, this $\mathcal{H}_{2,\Omega}$ problem has been attacked using the **DARPO** procedure [37, Chap. 8], a descent algorithm, and the **FL-ISTIA** procedure [39], involving frequency-limited gramian, taking advantage of a subset of the interpolation conditions (2.9). In the remainder of the paper, we will consider the **FL-ISTIA** procedure developed in [39].

3. Gust load–oriented modeling. Now that the rational approximation tools have been introduced, let us present the GLA problem as well as the first contribution: the exact gust

[2]Note that in [26], a similar procedure achieving first-order $\mathcal{H}_2$ optimality with interpolatory conditions with an input-output delayed **LTI** model has been developed.

load aeroelastic model definition. Figure 1 illustrates the considered feedback control loop architecture, where the sampled GLA function denoted as *GLA controller* is to be computed and validated. One may note that the actuators, sensors, *flight controller* (a priori fixed), and computational delay for the GLA function are considered as given and included in the considered generic business jet (BizJet) aircraft model set, referred to as $\{\mathbf{G}_i\}_{i=1}^{n_s}$, and detailed hereafter.

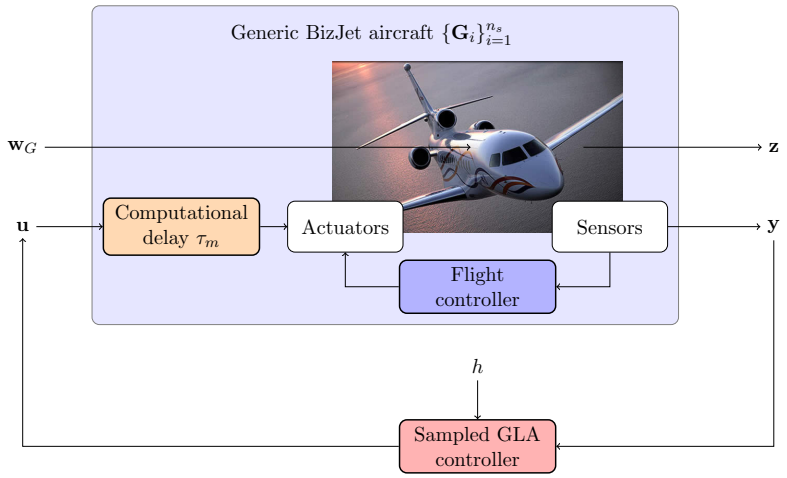

Figure 1. *Closed-loop architecture of the GLA problem. The complete aeroservoelastic dynamical aircraft models* $\{\mathbf{G}_i\}_{i=1}^{n_s}$ *include the "flight controller," "actuators," "sensors," and "computational delay* τ_m*." The "GLA controller" is the GLA function to be computed. Signals* $\mathbf{w}$*,* $\mathbf{u}$*,* $\mathbf{z}$*, and* $\mathbf{y}$ *denote the exogenous inputs, control inputs, performance outputs, and measurements, respectively. Then* h *denotes the sampling time for the GLA.*

The GLA problem is stated in subsection 3.1. In subsection 3.2, the large-scale aeroservoelastic models $\{\mathbf{G}_i\}_{i=1}^{n_s}$, as provided by physics and load teams, is described. Its input-output simplification is then done in subsection 3.3, leading to the set of irrational models $\{\mathbf{H}_i\}_{i=1}^{n_s}$.

3.1. GLA feedback control objective. An important aircraft design criteria concerns the *gust load envelope* that should not reach some limit to ensure structure integrity. To this aim, it is standard to consider vertical gusts $\mathbf{w}_g$, modeled through the so-called 1-cosine profile

$$\mathbf{w}_g(t) = \begin{cases} \dfrac{W}{2}\left(1-\cos\left(\dfrac{\pi V}{L}t\right)\right) & \text{for } 0 \le t \le \dfrac{2L}{V}, \\ 0 & \text{for } t > \dfrac{2L}{V}, \end{cases} \tag{3.1}$$

where W is the gust velocity (in feet), L is the gust wavelength (in meters), and V is the aircraft true airspeed (in meters per second).[3] The *gust load envelope* is simply the worst-case load response along the wingspan in reaction to the set of time-domain vertical wind gust profiles (3.1) affecting the aircraft. Similarly to aerodynamical effects inducing vibrations

[3]Typical values for these parameters are provided by authorities and result in hundreds of different gust configurations.

[23], these gusts represent typical phenomena the aircraft might face during its exploitation. Prior to any flight test, aircraft manufacturers should guarantee authorities that they are controlled. In the preliminary conception step (before considering any control functions), the aircraft is designed by experts so that the wings support a given nominal load envelope, dictated by physical considerations such as desired aircraft maneuverability, gust, and many other manufacturing constraints. The larger the supported loads are, the larger the structural stiffeners and mass reinforcements should be. The aircraft mass is consequently bigger and its consumption during flight increased. In this context, GLA control function plays an important role in the aircraft conception: It is aimed at lowering the load envelope and thus at reducing the aircraft's overall mass, consumption, and emissions [1]. In this work, the gain brought by the GLA on the *worst upward gain* is denoted by $\mathcal{E}(x_i)$ and is computed as

$$\mathcal{E}(x_i) = \max_{\mathbf{w}_g \in \mathcal{W}} \left\| \frac{\mathbf{z}_{\text{loads}}(x_i) - \mathbf{z}_{\text{loads}}^{(\text{GLA})}(x_i)}{\mathbf{z}_{\text{loads}}(x_i)} \right\|_\infty, \tag{3.2}$$

where x_i is the wing location points where the loads are computed (here five locations $x_i = [x_1, x_2, x_3, x_4, x_5]$) and where $\mathcal{W}$ is the set of gust profiles as in (3.1). Then $\mathbf{z}_{\text{loads}}(x_i)$ denotes the load at location x_i for the baseline aircraft, and $\mathbf{z}_{\text{loads}}^{(GLA)}(x_i)$ denotes the one when the GLA control function is activated. Responses are obtained when the aircraft model is fed by (3.1). This model is detailed in the what follows.

3.2. Aeroservoelastic aircraft modeling. To guarantee the safety and performance levels, the GLA function is developed using a very accurate environment and models, issued from aeroservoelastic modeling teams [28, 29]. Indeed, to target important load alleviation levels and important mass reduction, all the aircraft dynamics should be considered from the beginning of the study. From the authors' experience, this is mandatory to prevent unexpected behavior resulting from any prior simplification. The dynamical models involved are then obtained from high-fidelity aeroelastic and flow software. More specifically, the hereafter considered model set aggregates different blocks constructed by different teams, software, and experts. A finite element approach is used to obtain a model of the aircraft structure in the form of a finite-dimensional second-order model dynamic. It is then completed by the fluid, atmosphere, and actuator effects on the structure through a set of linear, polynomial, and rational functions, internal to the industrial process. The resulting model, detailed in what follows, is provided as a first-order **DAE** with multiple inputs and outputs (see also [29] and [18] for details).

Following Figure 1, $\{\mathbf{G}_i\}_{i=1}^{n_s}$ denotes the family of gust load–oriented dynamical models. Each $\mathbf{G}_i$ $(i = 1, \ldots, n_s)$ represents a *linear time invariant dynamical model* of the aircraft, evaluated at a given flight and mass condition. Its construction is a know-how of the aircraft manufacturer and usually results from multiple steps performed by different experts from fluid mechanics, structural, and test teams. Each transfer function $\{\mathbf{G}_i\}_{i=1}^{n_s}$ is described by the following realization denoted $\{\mathcal{G}_i\}_{i=1}^{n_s}$:

$$\dot{\mathbf{x}}^{(i)}(t) = A^{(i)}\mathbf{x}^{(i)}(t) + B^{(i)} \begin{bmatrix} \mathbf{w}_G(t) \\ \mathbf{u}(t) \end{bmatrix} \quad \text{and} \quad \begin{bmatrix} \mathbf{y}(t) \\ \mathbf{z}(t) \end{bmatrix} = C^{(i)}\mathbf{x}^{(i)}(t) + C_d^{(i)}\mathbf{x}^{(i)}(t - \tau_m), \tag{3.3}$$

where $\mathbf{x}^{(i)}(t) \in \mathbb{R}^{M_i}$, $\mathbf{u}(t) \in \mathbb{R}^{n_u}$, $\mathbf{w}_G(t) \in \mathbb{R}^{n_{wG}}$, $\mathbf{y}(t) \in \mathbb{R}^{n_y}$, and $\mathbf{z}(t) \in \mathbb{R}^{n_z}$ are the internal

variables, input, exogenous input, output, and performance output signals, respectively. The dimensions n_u, n_{wG}, n_y, and n_z are constant for all n_s models, while M_i depends on the model configuration. Finally, $\tau_m \in \mathbb{R}_+$ represents the delay for the GLA control law computation.

In the considered use case, $\mathbf{u}$ gathers three control inputs: the horizontal tail and the inner and outer ailerons ($n_u = 3$). Exogenous input $\mathbf{w}_G$ gathers $\delta^\star_{mc}$, the aircraft horizontal tail deflection given by the pilot, the gust disturbance, and its first and second derivatives, applied at three different locations of the aircraft fuselage ($n_{wG} = 10$). This vector reads

$$\begin{aligned}\mathbf{w}_G(t) = \Big[\delta^\star_{mc}(t), \underbrace{\mathbf{w}_g(t), \dot{\mathbf{w}}_g(t), \ddot{\mathbf{w}}_g(t)}_{\text{front of the aircraft}}, \underbrace{\mathbf{w}_g(t-\tau_1^{(i)}), \dot{\mathbf{w}}_g(t-\tau_1^{(i)}), \ddot{\mathbf{w}}_g(t-\tau_1^{(i)})}_{\text{middle of the aircraft}}, \dots \\ \underbrace{\mathbf{w}_g(t-\tau_2^{(i)}), \dot{\mathbf{w}}_g(t-\tau_2^{(i)}), \ddot{\mathbf{w}}_g(t-\tau_2^{(i)})}_{\text{rear of the aircraft}}\Big]^T,\end{aligned} \tag{3.4}$$

where the same gust (position, velocity, and acceleration) enters in the model at the front, the middle, and the rear, with a delay $\tau_1^{(i)} \in \mathbb{R}_+$ and $\tau_2^{(i)} \in \mathbb{R}_+$, depending on the aircraft velocity. The only considered measurement $\mathbf{y}$ is the aircraft angle of attack at the nose level ($n_y = 1$). Finally, the performance $\mathbf{z}$ gathers outputs being the tracking signal error between the load factor without ($\mathbf{n}_z^\star$) and with ($\mathbf{n}_z$) GLA controller $\mathbf{n}_z^\star - \mathbf{n}_z$ and the load envelope $\mathbf{z}_{\text{loads}}(x_i)$ ($n_z = 6$). The $A^{(i)}$, $B^{(i)}$, $C^{(i)}$, and $C_d^{(i)}$ matrices are real and of appropriate dimensions.

3.3. Toward gust load control–oriented models. As signals in (3.4) are repeated and linked together, it may be problematic to deal with in a control design setup. One solution is to merge them in order to deal with $\mathbf{w}(t) = [\delta^\star_{mc}(t), \mathbf{w}_g(t)]^T$ instead of (3.4). This can be obtained by applying the following transformation:

$$\begin{bmatrix} \delta^\star_{mc}(t) \\ \mathbf{w}_g(t) \\ \dot{\mathbf{w}}_g(t) \\ \ddot{\mathbf{w}}_g(t) \\ \mathbf{w}_g(t-\tau_1^{(i)}) \\ \dot{\mathbf{w}}_g(t-\tau_1^{(i)}) \\ \ddot{\mathbf{w}}_g(t-\tau_1^{(i)}) \\ \mathbf{w}_g(t-\tau_2^{(i)}) \\ \dot{\mathbf{w}}_g(t-\tau_2^{(i)}) \\ \ddot{\mathbf{w}}_g(t-\tau_2^{(i)}) \end{bmatrix} = \begin{bmatrix} 1 & 0 \\ 0 & 1 \\ 0 & s \\ 0 & s^2 \\ 0 & e^{-\tau_1^{(i)}s} \\ 0 & se^{-\tau_1^{(i)}s} \\ 0 & s^2e^{-\tau_1^{(i)}s} \\ 0 & e^{-\tau_2^{(i)}s} \\ 0 & se^{-\tau_2^{(i)}s} \\ 0 & s^2e^{-\tau_2^{(i)}s} \end{bmatrix} \begin{bmatrix} \delta^\star_{mc}(t) \\ \mathbf{w}_g(t) \end{bmatrix}, \tag{3.5}$$

where s denotes the Laplace variable. By merging (3.3) and (3.5), one can now reconstruct each model in a realization form $\{\mathcal{S}_i\}_{i=1}^{n_s}$ as

$$\begin{cases} E^{(i)}\dot{\mathbf{x}}^{(i)}(t) = A_0^{(i)}\mathbf{x}^{(i)}(t) + A_1^{(i)}\mathbf{x}^{(i)}(t-\tau_1^{(i)}) + A_2^{(i)}\mathbf{x}^{(i)}(t-\tau_2^{(i)}) + B_g^{(i)}\begin{bmatrix} \mathbf{w}(t) \\ \mathbf{u}(t) \end{bmatrix}, \\ \begin{bmatrix} \mathbf{y}(t) \\ \mathbf{z}(t) \end{bmatrix} = C_0^{(i)}\mathbf{x}^{(i)}(t) + C_1^{(i)}\mathbf{x}^{(i)}(t-\tau_m), \end{cases} \tag{3.6}$$

where $\mathbf{x}^{(i)}(t) \in \mathbb{R}^{N_i}$, $\mathbf{u}(t) \in \mathbb{R}^{n_u}$, $\mathbf{w}(t) \in \mathbb{R}^{n_w}$, $\mathbf{y}(t) \in \mathbb{R}^{n_y}$, and $\mathbf{z}(t) \in \mathbb{R}^{n_z}$ are the internal variables, input, exogenous input, output, and performance output signals, respectively. With this new form, n_u, n_y, and n_z are unaffected, while $n_w = 2$ (instead of 10 in (3.4)) and $N_i = M_i + 6$ due to the additional double derivative and delay structure added. The $E^{(i)}$, $A_0^{(i)}$, $A_1^{(i)}$, $A_2^{(i)}$, $B_g^{(i)}$, $C_0^{(i)}$, and $C_1^{(i)}$ matrices are real and of appropriate dimensions. Following (3.6), the gust load model is a set of transfer functions $\{\mathbf{H}_i\}_{i=1}^{n_s}$ from $\mathbf{u}$ and $\mathbf{w}$ to $\mathbf{y}$ and $\mathbf{z}$:

$$\mathbf{H}_i(s) = \left(C_0^{(i)} + C_1^{(i)} e^{-\tau_m^{(i)} s}\right) \left(sE^{(i)} - A_0^{(i)} - A_1^{(i)} e^{\tau_1^{(i)} s} - A_2^{(i)} e^{\tau_2^{(i)} s}\right)^{-1} B^{(i)}. \tag{3.7}$$

Remark 3.1 (about the internal delays $\tau_1^{(i)}$ and $\tau_2^{(i)}$, and the $E^{(i)}$ matrix rank). In the considered use case, the fuselage is subdivided into three patches. Consequently, the gust vertical displacement signal $\mathbf{w}_g(t)$ given in (3.1) enters the model at t, $t + \tau_1^{(i)}$ and $t + \tau_2^{(i)}$ ($0 < \tau_1^{(i)} < \tau_2^{(i)}$). To consider one single gust input signal (instead of three delayed), internal delays are added in the model. Similarly, to be able to accurately compute the loads along the wings, the model must take as gust input its vertical displacement as in (3.1) and its first and second derivatives as in (3.4) [29]. Once again, to reduce the number of input disturbances to one instead of three (position, velocity, and acceleration), the first and second derivatives of (3.1) are embedded in the model, leading to a descriptor form as in (3.6). More specifically, in our case, the $E^{(i)}$ matrix rank is then equal to $N_i - 6$: two rank loss per fuselage patch (one for the first and one for the second derivative). This descriptor form allows to decrease the number of input variables.

The BizJet use case is described by (3.6) and (3.7). However, these relations are not appropriate to manipulate in a control design objective for the following reasons: (i) The internal vector dimension of each model $\mathcal{S}^{(i)}$ is large (i.e., $N_i \approx 300$), leading to medium-scale matrices and a computational burden inappropriate with the control design; (ii) the presence of internal delays renders the model irrational and results in an infinite number of eigenvalues, for which dedicated tools exist but are complex to manipulate in an industrial context; and (iii) the $E^{(i)}$ matrix being rank deflective, computational tools are not always appropriate.

4. Interpolatory-driven aeroservoelastic aircraft gust load–oriented reduced modeling.

In this section, the irrational models presented in section 3 will be simplified through the interpolatory tools of section 2. The principal objective is to construct a control-oriented model for the GLA control design, simulation, and analysis. The following subsections 4.1 and 4.2 successively describe the exact continuous-time rational approximation and frequency-limited model order reduction of the aeroelastic business jet aircraft models. Numerical results are presented in subsection 4.3.

4.1. BizJet aircraft rational and polynomial approximation.

The first step of the process consists in replacing each infinite[4]-dimensional model $\mathbf{H}_i$ (3.7) by a finite-order rational one $\mathbf{H}_i^{n_i}$ of order n_i ($i = 1, \dots n_s$). By considering each n_s continuous-time model of the considered GLA use case, one can apply the rational approximation by interpolation using the method

[4]These models, embedding a state-space of order N_i are of infinite dimension due to the internal delays, leading to an infinite number of eigenvalues.

recalled in subsection 2.1. Then one obtains a set of n_s continuous-time rational approximated models $\{\mathbf{H}_i^{n_i}\}_{i=1}^{n_s}$ equipped with realization $\{\mathcal{S}_i^{n_i}\}_{i=1}^{n_s}$ with matrices as (2.6). Note that each of the n_s models may have a different dimension n_i, this latter being automatically computed by the rank condition given in (2.5). Here, the original models (3.7) are given in continuous time. A standard way consists in gridding the interpolation (support points) along the imaginary axis as it is related to the frequency response. In our case, for all configurations, the interpolating points have been selected as follows:

$$\{z_k\}_{k=1}^{2m} = \underbrace{\{\imath\omega_j, -\imath\omega_j\}_{j=1}^{m}}_{\{\mu_j\}_{j=1}^{m}} \cup \underbrace{\{\imath\nu_i, -\imath\nu_i\}_{i=1}^{m}}_{\{\lambda_i\}_{i=1}^{m}}, \tag{4.1}$$

where $\omega_j, \nu_i \in \mathbb{R}_+$ are the pulsations at which one evaluates each transfer $\{\mathbf{H}_i\}_{i=1}^{n_s}$, with $2m = 1000$. In our application, ω_j and ν_i are selected to be logarithmically spaced from 10^{-2} to 10^3. This choice allows to focus on the frequency range of interest. Indeed, in the case of irrational models, the method is efficient for interpolation but not necessary for extrapolation.

In addition, as the stability of the obtained rational model $\{\mathbf{H}_i^{n_i}\}_{i=1}^{n_s}$ is not guaranteed by the Loewner interpolatory procedure, a *poststabilization* is performed using the procedure presented in [19]. This latter consists in projecting the rational models $\{\mathbf{H}_i^{n_i}\}_{i=1}^{n_s}$ onto their closest stable model, here using the $\mathcal{H}_\infty$-norm, leading to a set of stable models of the same dimensions. Mathematically, given a realization $\mathcal{S}$ associated to $\mathbf{H} \in \mathcal{L}_\infty$, one aims at finding $P_\infty(\mathbf{H}) \in \mathcal{H}_\infty$ such that $P_\infty(\mathbf{H}) = \arg\inf_{\mathbf{G}\in\mathcal{H}_\infty} ||\mathbf{H}-\mathbf{G}||_{\mathcal{L}_\infty}$. Technical details and assumption can be found in [19]. Each model now shares a rational structure and is now stable and of finite order n_i for $i = 1, \ldots, n_s$. Note that here, the stability enforcement is performed since one knows that original models are structurally and physically stable. At this point, the delay terms are removed and traded with rational order model n_i, determined by (2.5).

Remark 4.1 (about a Padé delay approximation). It can be appealing to replace the delays with a Padé approximation, which preserves the gain but modifies the phase. While this is classically performed in many applications, it is, in the authors' experience, not the most accurate way of dealing with delays, as it leads to a significant error in the phase. In addition, the use of Padé will drastically increase the model internal vector. Therefore, the accuracy /complexity ratio is not in favor of Padé approximation.

4.2. BizJet aircraft control–oriented model reduction. As a second step and rooted on $\{\mathbf{H}_i^{n_i}\}_{i=1}^{n_s}$, the obtained continuous-time rational models, one now invokes again the *interpolatory framework* for a dimension reduction. Now we follow the approach detailed in subsection 2.4 to reduce the model over a frequency-limited range. For the considered application and in view of control design, it is important to reduce as much as possible the model while staying representative. Indeed, as the controller designed later is a solution of an optimization problem, the simpler the model is, the more efficient the optimization is.

In addition, as the GLA function should act in a given frequency range without altering the flight control laws, it is relevant to reduce the model over a frequency-limited range $[0, \omega]$ only (where $\omega \in \mathbb{R}_+$). The **FL-ISTIA** process [39] being also a fixed point procedure, its initialization is done by selecting starting interpolating points as follows (where $0 < \omega_k < \omega$

and $\omega_0 < \omega$):

$$\begin{aligned} \{\hat{\kappa}^{(0)}\}_{k=1}^{r} &= \{\imath\omega_k, -\imath\omega_k\}_{k=1}^{r/2} && \text{if } r \text{ is even,} \\ \{\hat{\kappa}^{(0)}\}_{k=1}^{r} &= \{\imath\omega_k, -\imath\omega_k\}_{k=1}^{\lfloor r/2 \rfloor} \cup \omega_0 && \text{if } r \text{ is odd.} \end{aligned} \tag{4.2}$$

4.3. Application to the BizJet models. As an illustration, Figure 2 compares the frequency and phase responses from the gust input to the wing root bending moment at 2 m from the fuselage of the original irrational model $\mathbf{H}_7$ with its rational approximations $\mathbf{H}_7^{n_7}$ and frequency-limited reduced model $\hat{\mathbf{H}}_7$ for one single configuration point. Sigma plot and mismatch errors are also reported in Figure 3. All other cases are similarly obtained.

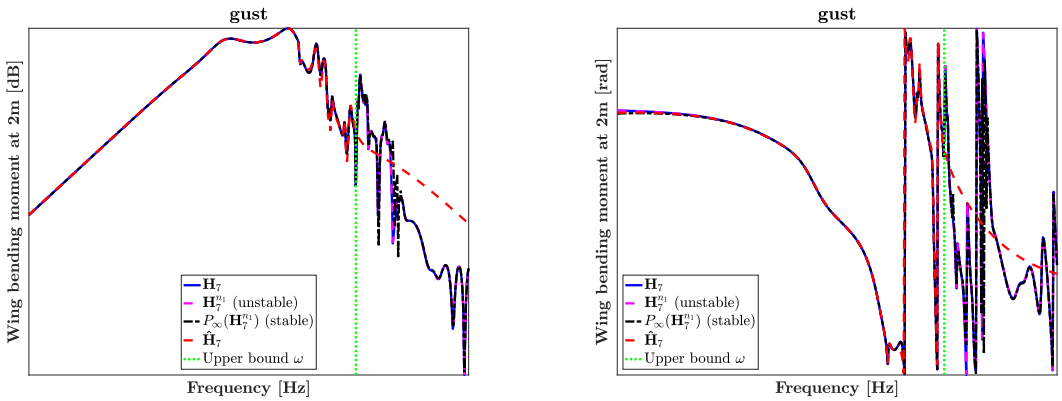

Figure 2. *Gain (left) and phase (right) frequency responses of the transfer from gust to the sizing wing root bending moment at 2 m from the fuselage: the original model $\mathbf{H}_7$ (solid blue line), the approximated and approximated plus projected stable models $\mathbf{H}_7^{n_7}$ (dashed magenta and dash dotted black lines, respectively), and the reduced-order model $\hat{\mathbf{H}}_7$ with dimension $r = 30$. Upper bound of the reduction frequency band is materialized by the vertical green dashed line.*

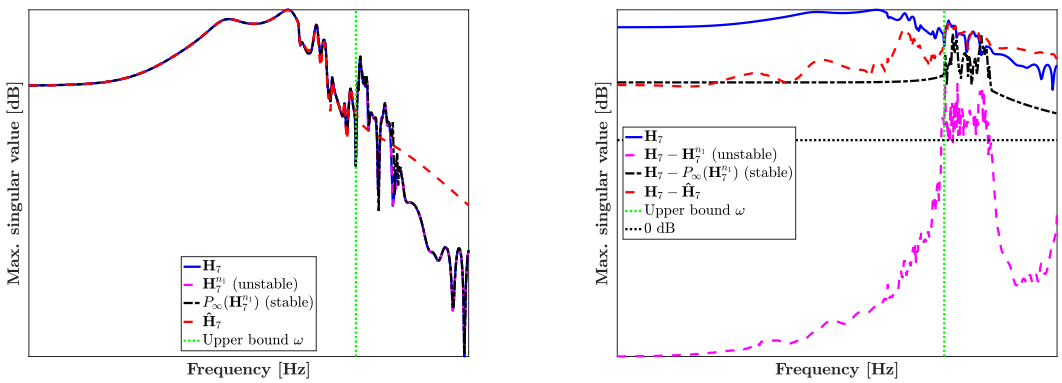

Figure 3. *Gain (left) and gain error (right) of the maximal singular frequency responses.*

With reference to Figures 2 and 3, the following comments can be done. First, the rational approximation, satisfying the tangential interpolatory conditions (2.4), allows to accurately

capture the descriptor delayed model (3.7) gain, phase, and sigma, with a simple rational function (here for the 7th use case, $n_7 = 211$). Note that the projection [19] performed afterward to force the model to be stable is also accurate. Second, the frequency-limited order reduction still preserves a good matching in the considered frequency range, with a rational model of dimension $r = 30$ only. Analyzing the bottom frame of Figure 3, the $\mathbf{H}_7 - \mathbf{H}_7^{n7}$ (unstable) mismatch is close to machine precision up to the upper frequency limit ω. When projecting to obtain a stable model, the $\mathbf{H}_7 - P_\infty(\mathbf{H}_7^{n7})$ (stable) mismatch results in a loss of accuracy, traded with the stability property. The reduced model $\hat{\mathbf{H}}_7$ clearly is accurate below the upper frequency bound and can be considered as simple but accurate enough for GLA control design.

5. Interpolatory-driven sampled-time GLA function computation. Based on the reduced-order models $\{\hat{\mathbf{H}}_i\}_{i=1}^{n_s}$, we are now ready to design the GLA control function. As this control law has to be implemented on an onboard computer sampled with a fixed step time $h \in \mathbb{R}_+$, a discrete-time controller is sought. In the rest of this section, we first present the context of discrete-time control design in subsection 5.1. Then the continuous-time $\mathcal{H}_\infty$-norm synthesis of $\mathbf{K}$ is briefly exposed in subsection 5.2. In subsection 5.3, the discretization problem is introduced and is solved in the *new interpolatory framework* in subsection 5.4, leading to Algorithm 5.1, being the major (and second) contribution of this paper.

5.1. Preliminary words on discrete- and continuous-time control design. In dynamical systems and control theory, the continuous-time and discrete-time domains coexist. While most of the tools available in one domain have a counterpart in the other, it is not unusual that a specific application requires to switch from one domain to the other. In particular, in the considered GLA control-oriented application, engineers start from a continuous-time physical model set $\{\mathbf{H}_i\}_{i=1}^{n_s}$, simplified by a reduced continuous-time one $\{\hat{\mathbf{H}}_i\}_{i=1}^{n_s}$. The latter is then used for the design of the GLA control law. To this aim, as illustrated schematically in Figure 4, three approaches can be conducted: (i) One may discretize the analog plants $\{\mathbf{H}_i\}_{i=1}^{n_s}$ and then design a discrete control-law $\mathbf{K}_d$ with the same sampling period h. (ii) Conversely, one may design an analog control-law $\mathbf{K}$ and then discretize it. (iii) Or, using dedicated techniques from sampled-data systems theory (see, e.g., [12, Chaps. 12 and 13]), one may directly synthesize $\mathbf{K}_d$ from $\{\mathbf{H}_i\}_{i=1}^{n_s}$.

While the direct nature of the latter method (iii) is appealing, it requires dedicated theoretical and numerical tools that are not as widespread as usual ones, especially in the industry where this approach would require their whole control design and analysis process to be rethought. For these reasons, one focuses here on the indirect methods that remain of practical interest and more specifically on the continuous controller, followed by a discretization. Performing in the other ways, i.e., discretizing the model and then synthesizing the controller, would lead to an inaccurate model response due to the low-frequency sampling imposed by the onboard computer.

For both indirect approaches, a discretization step is required. This may have a detrimental impact with respect to the expected dynamical behavior. In that context, the availability of an efficient discretization method is of particular interest. Here, an approach based on the *Loewner interpolatory framework*, described in section 2, is used. It offers an interesting alternative to usual discretization processes, as it enables to reach a better frequency and

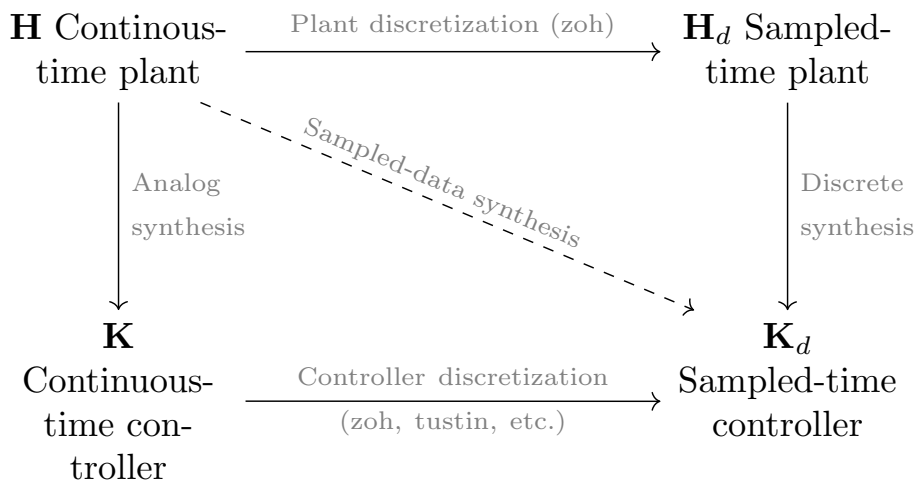

Figure 4. *Different paths to design a discrete control-law* $\mathbf{K}_d$ *from an analog plant* $\mathbf{H}$.

time-domain matching with the continuous-time description. Before detailing this approach, for sake of completeness, subsection 5.2 briefly presents the continuous-time GLA controller design.

5.2. Preliminary continuous-time GLA controller design. In the considered application, as the objective is to attenuate a worst-case amplification, the $\mathcal{H}_\infty$-norm minimization framework is clearly tailored. Being given the reduced continuous-time models $\{\hat{\mathbf{H}}_i\}_{i=1}^{n_s}$, the continuous-time controller $\mathbf{K}$, mapping outputs $\mathbf{y}$ to control inputs $\mathbf{u}$, as interconnected in Figure 1, is obtained by solving the following $\mathcal{H}_\infty$-norm problem for $i = 1, \dots \tilde{n}_s \leq n_s$:

$$\mathbf{K} = \arg \min_{\tilde{\mathbf{K}} \in \mathcal{K} \subseteq \mathcal{H}_2} ||\mathcal{F}_l(\mathbf{G}(\hat{\mathbf{H}}_i), \tilde{\mathbf{K}})||_{\mathcal{H}_\infty}, \tag{5.1}$$

where $\mathbf{G}(\hat{\mathbf{H}}_i) \in \mathcal{H}_\infty$ is the so-called generalized plant involving the input and output weight functions (not detailed here, as they are out of the scope of this paper) and the reduced-order models. Moreover, $\mathcal{F}_l(\cdot, \cdot)$ denotes the lower fractional operator. The control objective thus consists in finding the locally optimal continuous-time controller $\mathbf{K}$ such that (5.1) is solved, i.e., such that the $\mathcal{H}_\infty$-norm of the $\mathcal{F}_l(\mathbf{G}(\hat{\mathbf{H}}_i), \mathbf{K})$ loop, mapping exogenous inputs $\mathbf{w}$ to performance output $\mathbf{z}$, is minimized. In the considered case, one single measurement $\mathbf{y}$ is considered (the angle of attack at the front of the aircraft) with three symmetrical controllable movable surfaces (horizontal tail, inner and outer ailerons). The performance signals to be minimized are the sizing load output and the mismatch between the load factor without and with GLA (in order to preserve flight mechanics behavior). In addition, one seeks this controller such that it belongs to a subset $\mathcal{K} \subseteq \mathcal{H}_2$, reducing the controller search space to reduced-order structures without direct feed-through, avoiding issues for industrial implementation. The problem is solved by the routine developed by the authors of [6] and results in a stable moderate user-defined n_cth-order **LTI** continuous-time controller $\mathbf{K}$. When referring to (5.1), one notices that $\tilde{n}_s$ $\mathcal{H}_\infty$-norm problems are simultaneously solved, accounting for the different flight conditions.

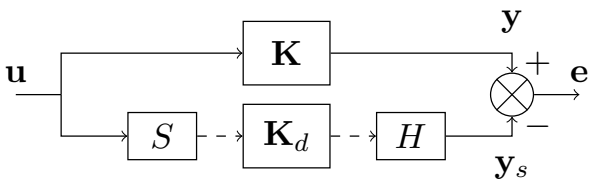

Figure 5. *Interconnection for the measurement of the discretization error between G and G_d.*

5.3. Controller discretization problem and discretization error derivation. Being given the linear continuous-time controller $\mathbf{K}$, the objective is to determine, for a fixed time step $h \in \mathbb{R}_+$, a discrete-time controller represented by the recurrence state-space equation $\mathcal{C}_d$,

$$\mathbf{x}_d[q+1] = A_d\mathbf{x}_d[q] + B_d\mathbf{y}_d[q] \quad \text{and} \quad \mathbf{u}_d[q] = C_d\mathbf{x}_d[q] + D_d\mathbf{y}_d[q], \tag{5.2}$$

where $\mathbf{x}_d[q] \in \mathbb{R}^{n_d}$, $\mathbf{u}_d[q] \in \mathbb{R}^{n_u}$, $\mathbf{y}_d[q] \in \mathbb{R}^{n_y}$ are the internal variables, sampled control, and measurements signals, respectively. One seeks for (5.2) such that (i) its associated transfer function $\mathbf{K}_d(z) = C_d(zI_{n_d} - A_d)^{-1}B_d + D_d$ is stable, i.e., $\mathbf{K}_d \in \mathcal{H}_\infty(\overline{\mathcal{D}})$, and (ii) the input-output behavior of $\mathbf{K}$ is well reproduced by $\mathbf{K}_d$ up to the Nyquist frequency. While discretization methods such as the bilinear (Tustin) one are clearly able to build a discrete-time model satisfying (i), the input-output behavior may be quite far from the original one when h is too large. Here, a method is proposed to build such a model by first using the *Loewner framework* to interpolate a specific set of frequency data and then, projecting the resulting model onto the stable subspace $\mathcal{H}_\infty(\overline{\mathcal{D}})$, to enforce sampled-time controller stability.

5.3.1. Measure of the discretization error. Quantifying the error induced by the discretization of $\mathbf{K}$ is not trivial. Indeed, the sampled nature of $\mathbf{K}_d$ prevents interconnecting it directly with the continuous $\mathbf{K}$ controller. Digital-to-analog converters are required. For a sampling time $h \in \mathbb{R}_+$, the latter are modeled here as the ideal sampler S and holder H. Then the error system is given by the interconnection of Figure 5, where discrete-time signals are represented by dashed lines. Such an interconnection of continuous- and discrete-time models is called a *sampled-data system* (**SD**).

The controller $\tilde{\mathbf{K}} = S\mathbf{K}_dH$ is no longer **LTI** but h-periodic, and consequently so is the error $\mathbf{K} - \tilde{\mathbf{K}}$, for which usual system norms cannot directly be applied. This problem has been addressed in the literature for direct **SD** synthesis (see, e.g., [7, 12]). The recurring idea is to use continuous lifting to transform a periodic system into a discrete-time **LTI** model with infinite input and output spaces on which equivalent $\mathcal{H}_2$ or $\mathcal{H}_\infty$ norms can be defined. While this framework appears well suited to evaluate $\mathbf{K} - \tilde{\mathbf{K}}$, the infinite dimensionality of the lifted model makes it quite technical. That is why here a more straightforward approach based on the *frequency characterization of the discretization error* formulated in [12, sect. 3.5] is considered instead. For that purpose, models for the ideal sampler and holder are recalled in subsection 5.3.2, and the frequency error is presented in subsection 5.3.3.[5]

[5]Note that in [12], the authors use the λ-transform, while here, one considers the z-transform; the sign of the exponential in the Fourier transforms of discrete signal is thus modified.

5.3.2. Ideal sampler and holder. Let us consider a continuous-time signal $v(t)$ and the sampling period h. The ideal sampler S transforms $v(t)$ into a discrete sequence $v_d[q]$ such that $v_d[q] = v(qh)$, $q \in \mathbb{Z}$. As shown in [12, Lem. 3.3.1], the Fourier transforms $\overline{v}_d = \mathcal{F}(v_d)$ and $\overline{v} = \mathcal{F}(v)$ are linked as follows:

$$\overline{v}_d(e^{\imath\omega h}) = \frac{1}{h}\sum_{q\in\mathbb{Z}} \overline{v}(\imath\omega + \imath q\omega_s), \tag{5.3}$$

where $\omega_s = 2\pi/h$ is the sampling frequency. Equation (5.3) highlights the frequency aliasing phenomena since all the multiples of the sampling frequency are indistinguishable in the output. Note that the sampling operator S is not bounded for any signal in $\mathcal{L}_2(\mathbb{R})$ as shown in [11]. To be bounded, the input signal v must be restricted to the class of band-limited $\mathcal{L}_2(\mathbb{R})$ signals, or it must be filtered by a finite-dimensional stable and strictly causal system, i.e., an antialiasing filter.

Similarly, the holder H transforms a sequence $v_d[q]$ into a continuous-time signal $v(t)$ such that $v(t) = v_d[q]$, where $qh \le t < (q+1)h$. The impulse response of the holder can be defined as the difference of two unit steps delayed by h. Let

$$R(s) = \frac{1 - e^{-sh}}{sh} \tag{5.4}$$

be the associated transfer function. Then, as shown in [12, Lem. 3.3.2], the Fourier transforms of v and v_d are linked as follows:

$$\overline{v}(\imath\omega) = hR(\imath\omega)\overline{v}_d(e^{\imath\omega h}). \tag{5.5}$$

Back to Figure 5, coupling (5.3) and (5.5) enables to express the frequency-domain relationship between $\mathbf{u}$ and $\mathbf{y}_s$ (for $|\omega| < |\omega_s|$):

$$\overline{\mathbf{y}}_s(\imath\omega) = R(\imath\omega)\mathbf{K}_d(e^{\imath\omega h})\sum_{q\in\mathbb{Z}} \overline{\mathbf{u}}(\imath\omega + \imath q\omega_s). \tag{5.6}$$

5.3.3. A frequency-domain error. Using (5.6), one can express the frequency-domain relationship between $\mathbf{u}$ and the discretization error $\mathbf{e} = \mathbf{y} - \mathbf{y}_s$ from Figure 5 as

$$\overline{\mathbf{e}}(\imath\omega) = \mathbf{K}(\imath\omega)\overline{\mathbf{u}}(\imath\omega) - R(\imath\omega)\mathbf{K}_d(e^{\imath\omega h})\sum_{q\in\mathbb{Z}} \overline{\mathbf{u}}(\imath\omega + \imath q\omega_s). \tag{5.7}$$

Assuming that $\mathbf{u}$ is band-limited, i.e., that $\overline{\mathbf{u}}(\imath\omega) = 0$ for $|\omega| > \omega_s/2 = \omega_N$, (5.7) becomes $\overline{\mathbf{e}}(\imath\omega) = \big(\mathbf{K}(\imath\omega) - R(\imath\omega)\mathbf{K}_d(e^{\imath\omega h})\big)\,\overline{\mathbf{u}}(\imath\omega)$. This readily suggests to consider

$$e_\infty(\mathbf{K}, \mathbf{K}_d) = \max_{\omega<\omega_N} \left|\mathbf{K}(\imath\omega) - R(\imath\omega)\mathbf{K}_d(e^{\imath\omega h})\right| \tag{5.8}$$

to quantify the discretization error. This frequency-domain characterization of the error inspired the novel discretization process presented in the next section. For the **MIMO** case, the absolute value in (5.8) may be replaced by the 2-norm.

5.4. Application of the Loewner framework for discretization. Now we are ready to describe the *interpolatory-driven discretization process* allowing to get $\mathbf{K}_d$ from the continuous-time controller $\mathbf{K}$.

5.4.1. Principle. Being given the considerations of subsection 5.3, let us consider the control transfer function $\mathbf{K} \in \mathcal{H}_\infty$ to be discretized at the sampling time h. Building a n_cth-order discrete-time model $\mathbf{K}_d$ that matches the input-output behavior of $\mathbf{K}$, the frequency-domain characterization of the discretization error (5.8) suggests that $\mathbf{K}_d$ must be such that

$$R(\imath\omega)\mathbf{K}_d(e^{\imath\omega h}) = \mathbf{K}(\imath\omega) \tag{5.9}$$

for $|\omega| < \omega_N$. Equation (5.9) represents an infinite number of interpolation conditions that may be approximated by sampling the interval $[0, \omega_N]$ such that, for $k = 1, \ldots, 2m$,

$$R(\imath\omega_k)\mathbf{K}_d(e^{\imath\omega_k h}) = \mathbf{K}(\imath\omega_k). \tag{5.10}$$

Such a model can be built by applying the *Loewner interpolation* framework recalled in subsection 2.1 to the following set of frequency data:

$$\left\{e^{\imath\omega_k h}, R(\imath\omega_k)^{-1}\mathbf{K}(\imath\omega_k)\right\}_{k=1}^{2m}, \tag{5.11}$$

where $e^{\imath\omega_k h}$ are the new interpolating points and $R(\imath\omega_k)^{-1}\mathbf{K}(\imath\omega_k)$ the new function to evaluate. With reference to (2.1), $e^{\imath\omega_k h}$ are the support points z_k. Then, by splitting them in the same ways, $R(\imath\omega_k)^{-1}\mathbf{K}(\imath\omega_k)$ represents the couple $\mathbf{v}_j^H$ and $\mathbf{w}_i$ (these variables are obtained by evaluating $R(\imath\omega_k)^{-1}\mathbf{K}(\imath\omega_k)$ at $e^{\imath\omega_k h}$ for $0 \leq \omega_k \leq \omega_N$, following (5.11)). With the notations of subsection 2.1, one obtains the mth-order $\mathbf{K}_d^m$ controller that can be lowered without loss of interpolatory accuracy to $\mathbf{K}_d^n$ ($n < m$). Obviously, should the order n_c be lower than the McMillan order n of the exact interpolating controller, then the interpolation conditions (5.10) will not be perfectly satisfied, but the controller will keep its dimension.

5.4.2. About the stability of the discretized model. When applied to the "hold" controller $R(\imath\omega_k)^{-1}\mathbf{K}(\imath\omega_k)$, the Loewner framework allows to construct a rational function in barycentric form that ensures interpolatory conditions at the support points z_k. However, no pole location control can be achieved. The singularities of the resulting interpolated controller depend on the support points ordering and/or singular value decomposition. Therefore, even if $\mathbf{K} \in \mathcal{H}_2$ (or $\mathcal{H}_\infty$), the transfer function $\mathbf{K}_d$ obtained via the process described above may not lie in $\mathcal{H}_\infty(\overline{\mathcal{D}})$, which is a major drawback in comparison to the bilinear of backward discretization schemes.

To overcome this issue, one can apply the same process as in [15] and as performed in subsection 4.1 (in continuous time). It consists in projecting the unstable model $\mathbf{K}_d$ onto $\mathcal{H}_\infty(\overline{\mathcal{D}})$ so that the $\mathcal{L}_\infty$-norm between $\mathbf{K}_d$ and its projection is minimized. This is the so-called Nehari problem, for which solutions have been given in the continuous-time domain [14] and in the discrete-time domain; see, e.g., [21]. Let us denote by P_∞ this projection operator so that if $\mathbf{K}_d \in \mathcal{L}_\infty(\partial\mathcal{D})$, then $P_\infty(\mathbf{K}_d) \in \mathcal{H}_\infty(\overline{\mathcal{D}})$ minimizes $\|\mathbf{K}_d - P_\infty(\mathbf{K}_d)\|_{\mathcal{L}_\infty}$.

Note that in the sampled-time case, the order of $P_\infty(\mathbf{K}_d)$ depends on the number of unstable poles of $\mathbf{K}_d$ and is lower than n_c when $\mathbf{K}_d$ is unstable. In particular, if $\mathbf{K}_d$ has n_+

Algorithm 5.1 Loewner-driven discretization.

Require: A continuous-time model $\mathbf{K} \in \mathcal{H}_\infty(\mathbb{C}_+)$, a sampling time $h > 0$, an upper bound $\bar{n}$ of the desired order, and a number m of interpolation points.

1: Sample the interval $]0, \omega_N[$ in $2m$ points ω_k
2: Evaluate $R(\imath\omega_k)^{-1}\mathbf{K}(\imath\omega_k)$
3: Apply Loewner to the data set (5.11) to get a first model $\mathbf{K}_d^m$ that matches all the data and get the underlying minimal McMillian order n
4: Set $r = \min(n, \bar{n})$
5: Reduce $\mathbf{K}_d^n$ to $\mathbf{K}_d^r$ using any interpolation method
6: Project $\mathbf{K}_d^r$ onto a stable subspace, i.e., compute the n_cth-order $\mathbf{K}_d = P_\infty(\mathbf{K}_d^r)$
7: **return** the model $\mathbf{K}_d \in \mathcal{H}_\infty(\overline{\mathcal{D}})$ of order $n_c \leq r \leq \bar{n}$

stable and n_- unstable poles and p is the multiplicity of the largest unstable Hankel singular value, then $P_\infty(\mathbf{K}_d)$ has order $n_+ + n_- - p$ (see [21]). To avoid this issue and for a numerically more robust approach, suboptimal projection methods may alternatively be considered (see, e.g., [19]).

Remark 5.1 (alternative approach). A similar problem can be considered using the $\mathcal{L}_2$-norm and is actually much easier to solve considering the decomposition $\mathcal{L}_2(\partial\mathcal{D}) = \mathcal{H}_2(\mathcal{D}) \oplus \mathcal{H}_2(\overline{\mathcal{D}})$. The solution is simply obtained by discarding the unstable part of the model. However, this solution has generally a greater impact on the frequency behavior of the model, which is not desirable here.

5.4.3. Loewner-driven discretization. The Loewner-driven discretization process, standing as the major theoretical contribution of this paper, is applied to the controller and is summarized in Algorithm 5.1. The following comments can be added:

- The reduction step from $\mathbf{K}_d^n$ to $\mathbf{K}_d^r$ (step 5) may also be achieved by standard model approximation techniques as the one presented in subsection 2.3 or, more interestingly, using the frequency-limited version of subsection 2.4. Then $\mathbf{K}_d^r$ should be projected on $\mathcal{H}_\infty(\overline{\mathcal{D}})$, and finally a stability preserving model reduction method could be used to obtain $\mathbf{K}_d$.
- As both $\mathbf{K}_d^r$ and $\mathbf{K}_d$ are easily available during the process, $\|\mathbf{K}_d^r - \mathbf{K}_d\|_{\mathcal{L}_\infty}$ can be evaluated to get an estimation of the discretization error $e_\infty(\mathbf{K}, \mathbf{K}_d)$ in (5.8).
- Similarly, when $r = \overline{n}$ (i.e., $\overline{n} < n$), computing $\|\mathbf{K}_d^n - \mathbf{K}_d^r\|_{\mathcal{L}_\infty} = \|\mathbf{K}_d^n - \mathbf{K}_d^{\overline{n}}\|_{\mathcal{L}_\infty}$ gives insights on whether the maximal allowed order $\overline{n}$ is enough to ensure a low error.
- If $\mathbf{K}_d^r$ is unstable, then step 6 leads to a loss of order (see subsection 5.4.2). Therefore, when $n_c < r$ (which is likely to happen[6]), r should be increased above $\bar{n}$ so that $P_\infty(\mathbf{K}_d)$ is of order $\bar{n}$, thus avoiding any loss of accuracy.

It should also be noted that Algorithm 5.1 does not exploit the state-space structure of $\mathbf{K}$ and only requires frequency data from it. Therefore, as presented in the preliminary work [38], the approach may be applied to a wider class of models than just those described by a state-space realization. Algorithm 5.1 is applied on the obtained continuous-time GLA con-

[6]Indeed, one tries to approximate data coming from an infinite-dimensional model by a rational one. A large-order r is generally required to achieve an exact interpolation.

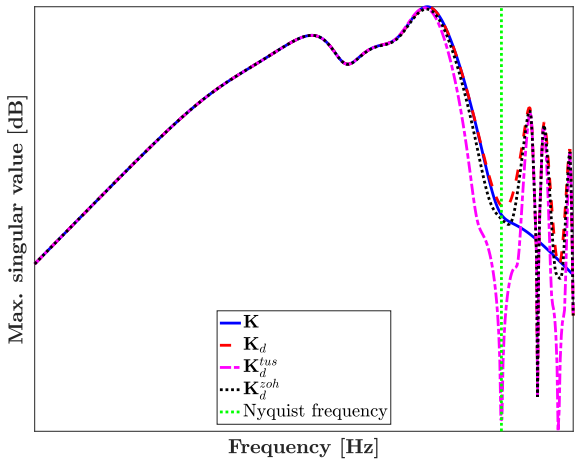

Figure 6. *Comparison of the sigma plot of different controllers: the continuous-time one* $\mathbf{K}$ *(solid blue line), the discrete-time one obtained with backward method* $\mathbf{K}_d^{zoh}$ *(dotted black line), the discrete-time one obtained with bilinear method* $\mathbf{K}_d^{tus}$ *(dash dotted magenta line), and the discrete-time one obtained with the interpolatory method* $\mathbf{K}_d$ *(dashed red line) including holder.*

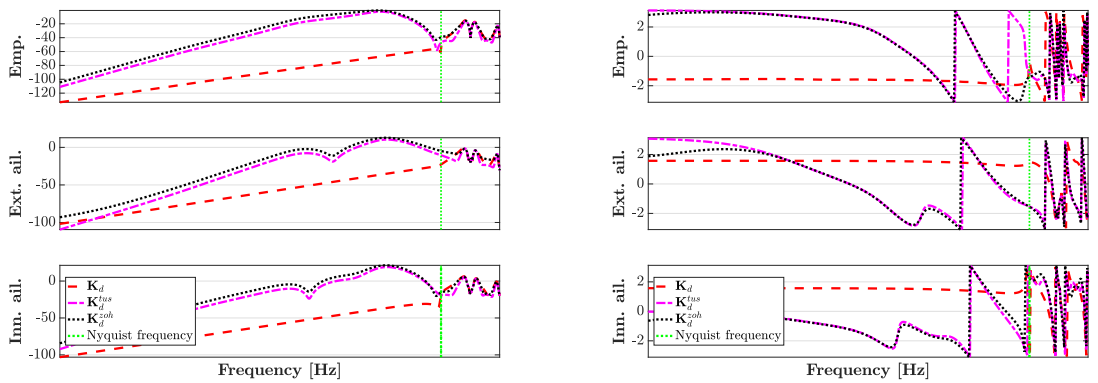

Figure 7. *Gain (left) and phase (right) errors: comparison of the Bode plot of all the controllers' transfers for different discretization methods with the continuous-time one* $\mathbf{K}$ *with holder. The discrete-time one obtained with backward method* $\mathbf{K}_d^{zoh}$ *(dotted black line), with bilinear method* $\mathbf{K}_d^{tus}$ *(dash dotted magenta line), and with interpolatory method* $\mathbf{K}_d$ *(dashed red line).*

troller. The obtained sampled-time controller sigma plot is shown in Figure 6, comparing the responses of the continuous-time controller $\mathbf{K}$ interconnected with a holder with different sampled controllers obtained with different methods (but same order n_c). Figure 7 reports the gain and phase mismatches that are obtained for each of the **SISO** transfers of the different sampled controllers.

With reference to Figures 6 and 7, one observes that the obtained $\mathbf{K}_d$ well reproduces the original controller $\mathbf{K}$ behavior up to the Nyquist frequency. The bilinear discretization

$\mathbf{K}_d^{tus}$ tends to compress the responses. Moreover, both bilinear and backward importantly modify the phase. This accurate restitution obtained by $\mathbf{K}_d$ is first justified by embedding the holder delay dynamics in the discretization and thus outperforms the classic ones. In addition, the Loewner interpolation allows to control the accuracy of the rational interpolant. More important effects on the closed loop will be presented in the conclusion in section 6.

6. Conclusions. In this paper, a complete end-to-end approach for the construction of a GLA control function has been presented, applied, and implemented on a real-life generic BizJet aircraft use case simulator, standing as another important contribution. As a conclusion to this paper, subsection 6.1 presents the obtained performances when plugging the discrete-time controller into the complete industrial simulator, including the time-delayed continuous-time model (hundreds of simulations are performed). As the proposed design scheme can be readily applied to any linear dynamical system and not only aircraft control, in subsection 6.2, we summarize the main methodological contributions.

6.1. BizJet aircraft GLA function performances. The main objective of GLA is to reduce the so-called load envelope, i.e., the load amplification along the wingspan in response to a gust signal family. This alleviation feature is presented in Figure 8 (left) for different discretized controllers, with the same dimension and sampling-time value h.

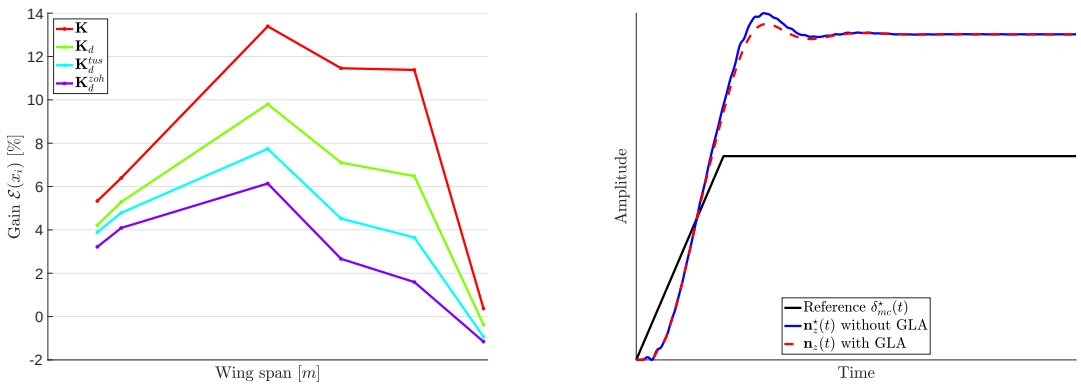

Figure 8. *Left: gust load attenuation envelope gain $\mathcal{E}(x_i)$ resulting to the interconnection presented in Figure 1 for different GLA controllers: the continuous-time one $\mathbf{K}$ (red line), the discrete-time are obtained with backward method $\mathbf{K}_d^{zoh}$ (purple line), with bilinear method $\mathbf{K}_d^{tus}$ (cyan line), and with the interpolatory method $\mathbf{K}_d$ (green line). Right: time-domain response of the interconnection Figure 1 without (solid blue line) and with (dashed red line) the GLA function to a pilot stick input (solid black line).*

While the "optimal" GLA level obtained by the continuous-time controller $\mathbf{K}$ leads to attenuation between 6% and 13% (except at the wingtip, where the loads are very small), the sampled-time versions with a sampling value h fixed by the available onboard computer clearly deteriorate the performances. Still, depending on the discretization method, one clearly observes an important gain when using the proposed discretization approach of Algorithm 5.1 with respect to the standard ones. In addition, the proposed load alleviation should not result in a change of flight performance. This is ensured by the control design and illustrated in

Figure 8 (right), where the normalized load factor variation in response to an elevator request $\delta^{\star}_{mc}(t)$ results in similar behaviors with and without the GLA function.

6.2. General contribution overview. The paper proposes an end-to-end solution to the GLA control design and implementation. This stands as the main contribution. The important load attenuation levels obtained result from (i) the use of an exact (and reduced) aeroservoelastic model including gust delays and derivative actions contribution and (ii) the development of a novel discretization method to discretize the controller. All the proposed steps are grounded on rational interpolatory methods. Indeed, the principal message of the article is to place *interpolatory methods* at the center of the modeling, design, and discretization steps. Moreover, even if centered on the discretization of the GLA function, Algorithm 5.1 provides a complete solution to discretize any linear dynamical model or controller. This last result provides an interesting alternative to the classical literature methods.

REFERENCES

[1] M. Alama, M. Hromcikb, and T. Hanis, *Active gust load alleviation system for flexible aircraft: Mixed feedforward/feedback approach*, Aerosp. Sci. Technol., 41 (2015), pp. 122–133.

[2] D. Amsallem and C. Farhat, *An online method for interpolating linear parametric reduced-order models*, SIAM J. Sci. Comput., 33 (2011), pp. 2169–2198.

[3] A. Antoulas, *The Loewner framework and transfer functions of singular/rectangular systems*, Appl. Math. Lett., 54 (2016), pp. 36–47.

[4] A. Antoulas, C. Beattie, and S. Gugercin, *Interpolatory Methods for Model Reduction*, SIAM Computational Science and Engineering, SIAM, Philadelphia, 2020.

[5] A. Antoulas, S. Lefteriu, and A. Ionita, *A tutorial introduction to the Loewner framework for model reduction*, in Model Reduction and Approximation Theory and Algorithms, P. Benner, A. Cohen, M. Ohlberger, and K. Willcox, eds., SIAM, Philadelphia, 2016, pp. 335–376.

[6] P. Apkarian and D. Noll, *Nonsmooth $\mathcal{H}_\infty$ Synthesis*, IEEE Trans. Automat. Control, 51 (2006), pp. 71–86.

[7] B. Bamieh, J. Boyd Pearson, B. Francis, and A. Tannenbaum, *A lifting technique for linear periodic systems with applications to sampled-data control*, Systems Control Lett., 17 (1991), pp. 79–88.

[8] L. Baratchart, *Existence and generic properties of L^2 approximants for linear systems*, IMA J. Math. Control Inform., 3 (1986), pp. 89–101.

[9] L. Baratchart, M. Cardelli, and M. Olivi, *Identification and rational $\mathcal{L}_2$ approximation: A gradient algorithm*, Automatica J. IFAC, 27 (1991), pp. 413–417.

[10] A. Bunse-Gerstner, D. Kubalinska, G.Vossen, and D.Wilczek, *h_2-norm optimal model reduction for large scale discrete dynamical MIMO systems*, J. Comput. Appl. Math., 233 (2010), pp. 1202–1216.

[11] T. Chen and B. Francis, *Input-output stability of sampled-data systems*, IEEE Trans. Automat. Control, 36 (1991), pp. 50–58.

[12] T. Chen and B. Francis, *Optimal Sampled-Data Control Systems*, Springer, New York, 1995.

[13] K. A. Gallivan, A. Vanderope, and P. Van Dooren, *Model reduction of MIMO systems via tangential interpolation*, SIAM J. Matrix Anal. Appl., 26 (2004), pp. 328–349.

[14] K. Glover, *All optimal Hankel norm approximation of linear multivariable systems, and their $\mathcal{L}_\infty$ error bounds*, Internat. J. Control, 39 (1984), pp. 1145–1193.

[15] I. Gosea and A. Antoulas, *Stability preserving post-processing methods applied in the Loewner framework*, in 2016 IEEE Workshop on Signal and Power Integrity, 2016, pp. 1–4.

[16] S. Gugercin, A. C. Antoulas, and C. A. Beattie, *$\mathcal{H}_2$ model reduction for large scale linear dynamical systems*, SIAM J. Matrix Anal. Appl., 30 (2008), pp. 609–638.

[17] N. Higham, *Accuracy and Stability of Numerical Algorithms*, 2nd ed., SIAM, Philadelphia, 2002.

[18] T. Klimmek, *Parametric set-up of a structural model for FERMAT configuration aeroelastic and loads analysis*, J. Aeroelasticity Struct. Dyn., 3 (2014), pp. 31–49.

[19] M. Kohler, *On the closest stable descriptor system in the respective spaces $\mathcal{RH}_2$ and $\mathcal{RH}_\infty$*, Linear Algebra Appl., 443 (2014), pp. 34–49.

[20] R. B. Lehoucq and D. C. Sorensen, *Deflation techniques for an implicitly restarted Arnoldi iteration*, SIAM J. Matrix Anal. Appl., 17 (1996), pp. 789–821.
[21] J. Mari, *Modifications of rational transfer matrices to achieve positive realness*, Signal Process., 80 (2000), pp. 615–635.
[22] A. J. Mayo and A. C. Antoulas, *A framework for the solution of the generalized realization problem*, Linear Algebra Appl., 425 (2007), pp. 634–662.
[23] C. Meyer, G. Broux, J. Prodigue, O. Cantinaud, and C. Poussot-Vassal, *Demonstration of innovative vibration control on a Falcon Business Jet*, in Proceedings of the International Forum on Aeroelasticity and Structural Dynamics, Como, Italy, June 2017.
[24] B. Patartics, G. Lipták, T. Luspay, P. Seiler, B. Takarics, and B. Vanek, *Application of structured robust synthesis for flexible aircraft flutter suppression*, IEEE Trans. Control Syst. Technol., (2021), pp. 1–15, https://doi.org/10.1109/TCST.2021.3066096.
[25] D. Petersson and J. Lofberg, *Model reduction using a frequency-limited $\mathcal{H}_2$-cost*, Systems Control Lett., 67 (2014), pp. 32–39.
[26] I. Pontes Duff, C. Poussot-Vassal, and C. Seren, *Optimal $\mathcal{H}_2$ model approximation based on multiple input/output delays systems*, Systems Control Lett., 117 (2018), pp. 60–67.
[27] C. Poussot-Vassal, *Large-Scale Dynamical Model Approximation and Its Applications*, HDR, habilitation thesis, Onera, INP Toulouse, Toulouse, France, 2019.
[28] M. Pusch, D. Ossmann, J. Dillinger, T. Kier, M. Tang, and J. Lubker, *Aeroelastic modeling and control of an experimental flexible wing*, in Proceedings of the AIAA Scitech 2019 Forum, 2019, 0131.
[29] D. Quero, P. Vuillemin, and C. Poussot-Vassal, *A generalized state-space aeroservoelastic model based on tangential interpolation*, Aerospace, 6 (2019), https://doi.org/10.3390/aerospace6010009.
[30] D. Quero, P. Vuillemin, and C. Poussot-Vassal, *A generalized eigenvalue solution to the flutter stability problem with true damping: The $p-L$ method*, J. Fluids Struct., 103 (2021), 103266.
[31] Y. Saad, *Iterative Methods for Sparse Linear Systems*, SIAM, Philadelphia, 2000.
[32] Y. Saad and M. Schultz, *GMRES: A generalized minimal residual algorithm for solving nonsymmetric linear systems*, SIAM J. Sci. Statist. Comput., 7 (1986), pp. 856–869.
[33] J. Spanos, M. Milman, and D. Mingori, *A new algorithm for $\mathcal{L}_2$ optimal model reduction*, Automatica J. IFAC, 28 (1992), pp. 897–909.
[34] P. Van Dooren, K. A. Gallivan, and P. A. Absil, *$\mathcal{H}_2$-optimal model reduction of MIMO systems*, Appl. Math. Lett., 21 (2008), pp. 53–62.
[35] P. Van Dooren, K. A. Gallivan, and P. A. Absil, *$\mathcal{H}_2$-optimal model reduction with higher order poles*, SIAM J. Matrix Anal. Appl., 31 (2010), pp. 2738–2753.
[36] C. D. Villemagne and R. E. Skelton, *Model reduction using a projection formulation*, Internat. J. Control, 40 (1987), pp. 2141–2169.
[37] P. Vuillemin, *Frequency-Limited Approximation of Large-Scale LTI Dynamical Models*, Ph.D. thesis, Onera, ISAE, Toulouse University, Toulouse, France, 2014.
[38] P. Vuillemin and C. Poussot-Vassal, *Discretisation of Continuous-Time Linear Dynamical Model with the Loewner Interpolation Framework*, preprint, arXiv:1907.10956, 2019.
[39] P. Vuillemin, C. Poussot-Vassal, and D. Alazard, *$\mathcal{H}_2$ optimal and frequency limited approximation methods for large-scale LTI dynamical systems*, in Proceedings of the 6th IFAC Symposium on Systems Structure and Control, Grenoble, France, February 2013, pp. 719–724.
[40] P. Vuillemin, C. Poussot-Vassal, and D. Alazard, *Spectral expression for the frequency-limited $\mathcal{H}_2$-norm of LTI dynamical systems with high order poles*, in Proceedings of the 13th European Control Conference, Strasbourg, France, June 2014, pp. 55–60.
[41] K. Willcox, J. Peraire, and J. White, *An Arnoldi approach for generation of reduced-order models for turbomachinery*, J. Comput. Fluids, 31 (2002), pp. 369–389.